Optimized shapes of oscillating resonators for generating high-amplitude pressure waves [a]

Xiaofan Li[b]

Department of Applied Mathematics, Illinois Institute of Technology

Chicago, IL60616

Joshua Finkbeiner[c], Ganesh Raman

Department of Mechanical, Materials and Aerospace Engineering, Illinois Institute of Technology Chicago, IL60616

Christopher Daniels

University of Akron

Akron, OH 44325

and

Bruce M. Steinetz

NASA Glenn Research Center

Cleveland, OH44135

Date: December 29, 2003

---

[a] Abbreviated title: Optimized resonator shapes

[b] Electronic mail: lix@iit.edu

[c] Current Address: NASA Glenn Research Center, Cleveland, OH44135

ABSTRACT

It is well known that the resonator geometry strongly influences the resonant frequencies of an acoustical resonator and the generated nonlinear standing pressure waveform. Maximizing the ratio of maximum to minimum gas pressure at an end of an oscillating resonator by optimizing the cavity contour is investigated numerically. A quasi-Newton type scheme is used to find optimized axisymmetric resonator shapes to achieve the maximum pressure compression ratio. The acoustical field is solved using a one-dimensional model, and the resonance frequency shift and hysteresis effects are obtained through an automation scheme based on continuation methods. Results are presented from optimizing cone, horn-cone, and cosine resonator geometries. Significant performance improvement is found in the optimized shapes over others previously published. Different optimized shapes are found when starting with different initial guesses, indicating multiple local extrema. The numerical model is validated by comparing with the experimental results of a horn-cone shaped resonator.

PACS numbers: 43.25.Gf, 43.25.Cb

I. INTRODUCTION

The waveform of the standing wave in an oscillating closed cavity is strongly influenced by the geometry of the resonator cavity. It is well known that shocks form in a cylindrical tube when the interior gas is oscillating at its resonant frequency. Lawrenson *et al.*[1] at MacroSonix Corp first exploited the shape dependence and obtained high-amplitude and shock-free acoustic pressures in axisymmetric tubes of varying cross sections, referred to as resonant macrosonic synthesis (RMS). Peak acoustic pressures that measure three to four times ambient pressure and maximum to minimum pressure ratios of 27 were observed in shaped cavities. The size of the demonstrated overpressure reached the level that is required by commercial applications such as acoustic pumps or compressors. The researchers considered these types of axisymmetric shapes: cylinder, cone, hone-cone, and bulb. They concluded that the hone-cone resonator shape generated the highest overpressure for a given input power. They also demonstrated that the overall characteristics of the waveform does not change when a resonator is filled with different gases.

A companion paper by Ilinskii *et al.*[2] developed a one-dimensional frequency-domain model for studying the RMS numerically. The results confirmed the nonlinear standing waveform and the related characteristics such as shape-induced resonance hardening and softening observed in the experiments by Lawrenson *et al.*[1] To account for the energy losses in the boundary layer along cavity wall, Ilinskii *et al.*[3] later modified the one-dimensional model by introducing an additional term in the continuity equation and used a turbulence model. Hamilton *et al.*[4] analytically investigated the relationship between the natural frequency of a nonlinear

acoustic resonator and its shape as well as the nonlinear interactions of modes in the resonator. Chun and Kim[5] numerically investigated cosine shaped resonators in addition to cylindrical and conical shapes using high-order finite-difference approximations. They concluded that the half cosine-shape is more suitable to induce high compression ratio than other shapes under certain assumptions. Recently, Erickson and Zinn[6] used the Galerkin method to solve the one-dimensional model and found a non-monotonic increase in compression ratio when the flare constant is raised for a class of horn-shaped resonators. To serve commercial needs, such as in acoustic gas compressor and acoustic liquid pump, the objective is to find an optimized shape for generating higher overpressure. However, the optimization procedure and results have not yet been discussed.

In this article, the numerical schemes are introduced and the results are presented for optimizing the shape parameters that yield the highest maximum-to-minimum pressure ratio in each of the following resonator shapes: cone, horn-cone, and cosine-shape. In Sec. II, the modeling equations are presented; in Sec. III, the numerical schemes are described; in Sec. IV, the numerical model and experiment results are compared and the resulting optimized shapes are discussed.

II. GOVERNING EQUATIONS

In this section, the one-dimensional model for computing the acoustic wave field in an axisymmetric resonator is briefly described. The equations are presented for completeness and the details of the derivation are given in the work by Ilinksii *et al.*[2].

Consider the acoustic field in an oscillating resonator of length l driven by an external force. The resonator is axisymmetric with the inner radius given by $r=r(x)$, $0<x<l$, where x is the coordinate along the axis of symmetry.

The density of the gas ρ, the velocity u, and the pressure p satisfy the conservation of mass

$$\frac{\partial \rho}{\partial t}+\frac{1}{r^2}\frac{\partial}{\partial x}\left(r^2\rho u\right)=0, \tag{1}$$

and the conservation of momentum

$$\frac{\partial u}{\partial t}+u\frac{\partial u}{\partial x}=-\frac{1}{\rho}\frac{\partial p}{\partial x}-a(t)+\frac{(\xi+4\eta/3)}{\rho}\frac{\partial}{\partial x}\left(\frac{1}{r^2}\frac{\partial}{\partial x}\left(r^2 u\right)\right), \tag{2}$$

where $a(t)$ is the acceleration of the resonator enforced by the external force; ξ and η are coefficients of viscosity. η is the shear viscosity, and ξ is the bulk viscosity that results from nonequilibrium deviations between the actual local pressure and the thermodynamic pressure. The state equation is specified by that of an ideal gas

$$p = p_0\left(\rho/\rho_0\right)^{\gamma}, \tag{3}$$

where p_0 is the ambient pressure, ρ_0 is the density, and γ is the ratio of specific heats of the gas. The no-penetration boundary conditions at the two ends require that the velocity vanish at $x=0$ and l.

The quasi-one-dimensional compressible Navier-Stokes equations (1)-(3) can be solved using different numerical methods. Instead of finite difference method or finite element method, the frequency-domain method is employed, where the unknown variables are expressed in terms of finite Fourier series in time and the Fourier coefficients are solved for. Both the experimental

and numerical results show that the time harmonics of the dependent variables, such as the pressure p, decay rapidly as the frequency increases. This ensures that the number of time harmonics, N, needed for accurate results is small. In our numerical simulations, we have set the value of N to be ten and found that increasing N does not change our results.

Following Ilinksii *et al.*[2] by expressing the variables in Fourier series, the Eqs. (1) and (2) can be reduced to a system of Ordinary Differential Equations (ODEs) for the Fourier coefficients of the velocity potential φ, defined as $u = \nabla\varphi$:

$$\begin{cases} \dfrac{d\hat{\varphi}_k}{dx} = \dfrac{\hat{v}_k}{r^2}, \\ \displaystyle\sum_l D_{kl} \frac{d\hat{v}_l}{dx} = f_k, k = 1,2,...,N \end{cases} \tag{4}$$

where $v = r^2 \dfrac{\partial\varphi}{\partial x}$, and $\hat{\varphi}_k$, $\hat{v}_k$ and $\hat{a}_k$ are the Fourier coefficients defined as $\varphi = \sum_{k=-N}^{N} \hat{\varphi}_k e^{ikt}$, $v = \sum_{k=-N}^{N} \hat{v}_k e^{ikt}$, $a = \sum_{k=-N}^{N} \hat{a}_k e^{ikt}$. The detailed expressions for $D_{kl} = D_{kl}(\hat{v}_k, \hat{\varphi}_k, x)$ and $f_k = f_k(\hat{v}_k, \hat{\varphi}_k, x)$ are given by

$$D_{kl} = \left(c_0^2 + ik\delta\right)\delta_{kl} + D'_{k-l},$$

$$f_k = -k^2 r^2 \hat{\varphi}_k + ikr^2 x\hat{a}_k + \frac{ik[v^2]_k}{r^2} + \sum_{l=-N+k}^{N} \hat{a}_{k-l}\hat{v}_k - \frac{\dfrac{dr^2}{dx}}{r^6} \sum_{l=-N+k}^{N} [v^2]_{k-l}\hat{v}_k,$$

where $\delta = \dfrac{\zeta + 4\eta/3}{\rho_0}$ is the viscosity, $c_0 = \sqrt{\dfrac{\gamma p_0}{\rho_0}}$ is the reference speed of sound, D'_m is given by $D'_m = -(\gamma - 1)x\hat{a}_m - im(\gamma - 1)\hat{\varphi}_m - \dfrac{\gamma + 1}{2r^4}[v^2]_m$, and $[v^2]_k = \sum_{l=-N+k}^{N} \hat{v}_{k-l}\hat{v}_l$. The no-slip boundary

conditions at the two ends are translated to the equivalent conditions in Fourier space: $\hat{v}_k = 0$ at $x = 0, l$.

After the Fourier coefficients $\{\hat{\varphi}_k\}$ and $\{\hat{v}_k\}$ are obtained by solving the boundary-value problem Eq.(4), the velocity potential φ and the modified velocity v are computed from the inverse FFT. The density ρ is given by the momentum equation

$$\frac{\rho}{\rho_0} = \left(1 - \frac{\gamma - 1}{c_0^2}\left[\frac{\partial \varphi}{\partial t} + \frac{1}{2r^4}v^2 + ax - \frac{\delta}{r^2}\frac{\partial v}{\partial x}\right]\right)^{\frac{1}{\gamma - 1}}, \tag{5}$$

and the pressure p can be obtained from the state equation (3).

III. NUMERICAL METHODS

In this section, the procedures for finding the optimal shape parameters are described so that the desired pressure waveform can be obtained. The overall steps are as follows: first, given a resonator shape and a fixed value of input power, the resonant frequency of the resonator is searched and the compression ratio, defined as the maximum-to-minimum pressure ratio at the narrow end, is computed; second, the optimization step is performed, which yields the next candidate for the optimal resonator shape; then, the first and the second steps are repeated until an optimal design is reached.

To simplify the discussion, the following dimensionless variables are introduced,

$$X = \frac{x}{l}, \quad T = \omega t, \quad R = \frac{r}{l}, \quad R_0 = \frac{r_0}{l}, \quad A = \frac{a}{l\omega_0^2}, \tag{6}$$

where ω is the frequency of the periodic force acted on the resonator, $\omega_0 = \pi c_0 / l$ is the fundamental frequency of a cylindrical resonator of length l.

In this work, the acceleration of the resonator induced by external force is assumed to be harmonic, $A(T) = \tilde{A}\cos(T)$. The physical parameters that determine the acoustic wave field in the resonator are: the acceleration amplitude $\tilde{A}$, the ratio of specific heats γ, the attenuation coefficient $G = \frac{\pi(\zeta + 4\eta/3)\omega_0}{c_0^2 \rho_0}$, and the resonator oscillating frequency $\Omega = \frac{\omega}{\omega_0}$.

A. Shape optimization

Suppose the resonator shape *R(X)* is determined by a number of shape parameters, $S_0, S_1, ..., S_n$. For example, a cone is given by $R(X) = S_0 + S_1 X$. The goal is to find the best shape producing the highest value of the pressure compression ratio R_c, which is defined as the ratio of maximum pressure to the minimum pressure at the narrow end of the resonator, i.e.,

$$R_c(S_0, S_{1,...,} S_n) = \frac{p_{\max}}{p_{\min}}, \text{ at } X=0. \tag{7}$$

The compression ratio R_c is a function of the shape parameters, the dimensionless frequency Ω, and the history of Ω (due to the existence of hysteresis effects). The method for obtaining R_c for a fixed resonator shape is explained later in the section.

Now, the method for finding the optimal resonator shape is presented. First, the practical conditions and constraints in the optimization are specified. The original experiments by Lawrenson *et al.*[1] and some commercial applications use refrigerant R-134a as the gas inside resonators. We set the specific heat ratio $\gamma = 1.2$ in order to match the gas properties of the refrigerant. The viscosity-related parameter G is fixed at 0.01, and will be shown later to be the value that makes the results from our numerical model match with those from the physical experiments. This same value of G was found appropriate in the study of Illinski[2]. For the current optimization, the dimensionless radius of the resonator at the narrow end, $R(X = 0)$, is restricted to be greater than 0.020833 so that real resonators could be built using these optimized dimensions.

The objective of the optimization is to maximize the compression ratio that would be observed in a real oscillating acoustic resonator. The electrodynamic shaker system used in this study and others[1,6] has limited acceleration capacity that is reduced by adding weight to the resonator. If we used the constraint to be constant acceleration amplitude, the optimization scheme would predict an optimum conical resonator shape that has a very small narrow end and very large wide end[7], resulting in heavy weight experimental hardware. However, in an experimental setup, this resonator would not produce high compression ratios due to the low acceleration generated by the shaker. A greater compression ratio would be obtained from lighter weight hardware oscillated at higher acceleration amplitude. Therefore, the amount of input power that is delivered to the resonator oscillation is fixed during the optimization, effectively favoring lighter weight resonators and more closely modeling the real system.

For a fixed amount of input power W_I, the acceleration amplitude $\tilde{A}$ from the mass of the resonator is deduced through the formula in dimensional variables

$$\langle W_I \rangle = (p_0 \omega l) \frac{1}{\pi} M \tilde{A}^2, \tag{8}$$

where M is the dimensionless mass of the resonator. Assuming the width and the density of the resonator wall are constant, the mass of the resonator M is proportional to the total surface area of the resonator. Equation (8) can be derived by assuming that most of the power consumed, $<W_I>$, is due to the inertial force F required to oscillate the resonator at the frequency ω. In dimensional variables,

$$\langle W_I \rangle = \frac{4}{T_p} \int_0^{T_p/4} Fu \, \mathrm{d}t = \frac{4}{T_p} \int_0^{T_p/4} mau \, \mathrm{d}t = \frac{4}{T_p} \int_0^{T_p/4} m \frac{\mathrm{d}u}{\mathrm{d}t} u \, \mathrm{d}t = \frac{2}{T_p} mu^2 \Big|_{t=0}^{T_p/4}, \tag{9}$$

where T_p is one period of the oscillation. Equation (8) follows as the dimensionless velocity of the resonator is given by $\tilde{A} \cos T$ and the power is nondimensionalized by $p_0 \omega l$.

Second, a quasi-Newton method, BFGS (Broyden-Fletcher-Goldfarb-Shanno[8]), is used for maximizing the multi-variable nonlinear function $R_c(S_0, S_{1,\ldots,} S_n)$. Since the evaluation of the objective function R_c itself involves solving a nonlinear system of ODEs, Eq. (4), many times, the gradient information of R_c required for the BFGS method is not available analytically and is derived by partial derivatives using a numerical differentiation method via finite differences. This entails perturbing each design variables, S_i, in turn and calculating the rate of change in the objective function $R_c(S_0, S_{1,\ldots,} S_n)$. For two shape parameters, the optimization takes 4 to 48 hours

of CPU time (depending on the type of the resonator shape and initial guess for the shape parameters) on a 1.3GHz Athlon T-Bird PC with the Lahey-Fujitsu FORTRAN compiler.

B. Boundary value problem

For a given shape of the resonator, the boundary value problem Eq. (4) is solved numerically by a Multiple Shooting Method. Since the amplitude of the pressure in a resonator strongly depends on the oscillating frequency Ω, the quantity to be optimized is the maximum pressure compression ratio R_c over the entire range of Ω for a given resonator shape. Because of the hysteresis effects, the solution is *not* unique near the resonant frequency and the Multiple Shooting Method will not converge unless a good initial guess of the solution is provided. To circumvent the difficulty, a continuation method is implemented: the system of ODEs is solved starting from a frequency Ω that is far away from the resonant frequency and the solution is used as an initial guess for solving the ODEs for increased or decreased Ω; the steps are repeated until all branches of the solution for all values of Ω near the resonance is completed. The maximum ratio R_c among different values of Ω is chosen as the compression ratio for the resonator.

IV. RESULTS

A. Characteristics of the standing waves

Before presenting the results of the optimal resonator's shapes, some of the important properties of the pressure wave in a non-cylindrical resonator are illustrated.

The horn-cone resonator shape is described by:

$$R(X) = \begin{cases} S_0 \cosh(S_1 X), & \text{for } 0 \le X \le S_2 \\ \alpha + \beta X, & \text{for } S_2 \le X \le 1 \end{cases} \tag{10}$$

where $S_0 = 0.028333, S_1 = 5.7264, S_2 = 0.25, \alpha = S_0 \cosh(S_1 S_2)$, and $\beta = S_0 S_1 \sinh(S_1 S_2)$. The shape parameters for the horncone are obtained from those used in the experiments by Lawrenson *et al.*[1]

In Fig.1, the pressure waveforms at the ends of a cylindrical resonator and the horncone resonator are shown at their corresponding resonance frequencies for the effective viscosity G–0.01, the gas specific heat ratio γ=1.2, and the acceleration $\tilde{A} = 1 \times 10^{-3}$. Throughout this paper, the effective viscosity G and the gas specific heat ratio are held constant. At the same acceleration magnitude, the waveform at the narrow end of the horncone shows large variation in which the ratio of the maximum and minimum pressure, R_c, exceeds the value of 30.5. On the other hand, the waveform for the cylinder shows the formation of shocks at resonance and the compression ratio R_c is below 1.32. The difference in the waveforms shows the strong dependence of the acoustic field on the geometry of a resonator. The graph also shows that the variation in pressure at the wide end of the horncone is much milder than that of the narrow end, oscillating within 23% above or below the value of the reference pressure p_0.

The ratio of the amplitudes of the second and the first harmonics of the pressure, p_2 / p_1, is plotted in Fig. 2 against the reduced amplitude of the first harmonic, p_1 / p_0, measured at one end of the cylinder and at the narrow end of the horncone. The figure shows that the second harmonic reaches its maximum at small amplitude of the first harmonic for the consonant (cylinder) resonator; however the second harmonic pressure increases more slowly than the first

harmonic for the dissonant (horncone) resonator. This indicates that the energy is contained in the first harmonic in the horncone resonator, thereby creating a large-amplitude pressure wave in the dissonant resonator. In contrast, the energy is efficiently transferred in a cylindrical resonator from lower to higher harmonics of pressure at relatively low total pressure amplitudes, thereby preventing the formation of large-amplitude pressure waves.

The amplitude of the first harmonic corresponding to the pressure in the horncone resonator is plotted against the frequency of the oscillating resonator in Fig. 3 for two different levels of acceleration, $\tilde{A} = 2\times10^{-4}$ and $\tilde{A} = 1\times10^{-3}$. For the smaller acceleration, the pressure is uniquely determined at each frequency; for the larger drive amplitude, the pressure takes one of the multiple values near the resonance, depending on the direction of the change in frequency. The existence of hysteresis and hardening resonance in horncone resonators requires that the largest pressure compression ratio be obtained through an upward frequency sweep. The numerical simulations show that the frequency increment size near the resonance must be small for the convergence of the Multiple Shooting method.

B. Comparison with experiments

While the numerical model by itself provides insight into the physics of the nonlinear acoustic standing waves in oscillating resonators, experimental verification is required to ensure that the model behaves as expected. Experimental data is used to generate the inputs to the numerical model. The result of the numerical simulation is then compared to the data gathered from the experiment.

The acceleration input to the numerical model is generated using measured signals from the experimental data. Recall that the model assumes that the resonator is excited using a simple sinusoidal acceleration. In addition, the resonator is assumed to be ideally rigid so that the acceleration is constant across the length of the resonator body. The arguments made in Finkbeiner *et al.*[9] allow the measured acceleration signals to be input to the model by isolating the fundamental acceleration harmonic as the driving function for the model.

The effective viscosity parameter G was originally unknown. The value for G is based in part upon the second coefficient of viscosity, due to the high-pressure gradients and frequencies present in the acoustics. Previous work[2] assumed a value of $G = 0.01$, although no justification was given for this value. To estimate this parameter, the pressure from the model computed for several different values of G, and the results for the varying values of G are then plotted together with the experimental data to determine the best match.[10]

In this study, a single comparison between experimental and numerical data is presented as an example of the procedure used. The experimental configuration is shown in Fig. 4. A horn-cone resonator is rigidly mounted wide-end down on a Labworks ET-127 shaker system. The shape of this resonator is given by Eq. (10) with the shape parameters $S_0 = 0.028333$, $S_1 = 5.7264$, and $S_2 = 0.25$.

PCB Piezotronics 353B03 accelerometers are mounted at both ends of the resonator. PCB Piezotronics dynamic pressure transducers are mounted in the sidewall of the resonator at axial positions of $X = 0.05$ and $X = 0.95$. Druck PDCR 130 static pressure transducers and thermocouples are mounted at the same axial positions as the dynamic pressure transducers (see Fig. 4). The dynamic transducers are optimized for high frequency pressure measurements and

are incapable of measuring static pressures due an exponential decay in voltage. The static transducers are used to measure this static value and complete the pressure measurement.

Several acceleration levels are used to excite the resonator; for the purposes of this study, an acceleration amplitude of roughly 50 g measured at the narrow end of the resonator is presented. At the acoustic resonance of the working fluid, the acceleration signals measured near the two ends have small difference in amplitude as graphed in Fig. 5. The dimensionless acceleration based on the signal measured at the wide and the narrow ends of the resonator is given by $\tilde{A} = 9.76 \times 10^{-5}$ and $\tilde{A} = 1.03 \times 10^{-4}$ respectively. The difference in the amplitude at the two ends is due to elasticity of the resonator. The dynamic pressure frequency response measured at the narrow end of the horn-cone resonator is displayed in Fig. 6 along with the curves which are computed for varying values of G with a dimensionless acceleration level, $\tilde{A} = 1.03 \times 10^{-4}$, matching the acceleration measured at the resonator narrow end. The computational pressure amplitude is measured at the axial location of $X = 0.05$. The result shows that the model over-predicts the resonant frequency of the horn-cone resonator by roughly 2.6%. However, in terms of amplitude and wave form, the model predicts the pressures generated in the resonator very well. The matching value of G is between 0.011 and 0.012 with acceleration referenced at the narrow end. Similar comparison shows, when the computed pressure frequency response curves are calculated based on the dimensionless acceleration at the narrow end, $\tilde{A} = 9.76 \times 10^{-5}$, the matching value of G is found to lie in (0.010, 0.011). These values of G are, for all intents and purposes, close to those assumed in previous studies[2].

C. Optimal conical shapes

In following subsections, the results are shown from optimizing each type of resonator shapes to achieve maximum compression ratio R_c at one end of the resonators. Again, in the optimization process the ratio of specific heats is held at γ=1.2, the attenuation coefficient G=0.01. The acceleration $\tilde{A}$ for a given shape is calculated from Eq. (8), where the value of the fixed input power is deduced from that for a reference conical resonator accelerated at the amplitude $\tilde{A} = 5\times10^{-4}$. The conical resonator contour can be written as

$$R(X) = S_0 + S_1 X, \text{for } 0 \le X \le 1 \tag{11}$$

The conical resonator studied in Lawrenson *et al.*[1] and Ilinksii *et al.*[2] with S_0=0.032941 and S_1=0.26800 is chosen to be the reference resonator. For the reference resonator, the compression ratio reaches its maximum value of $R_c = 5.0475$ when the oscillation frequency is raised to $\Omega = 1.3134$.

Using the optimization procedure described in Sec. III and starting with the reference conical shape, the optimal conical resonator is found to have the shape parameters $S_0 = 0.020833$ and $S_1 = 0.15438$. The compression ratio R_c of the conical resonator reaches a value of 6.7213, which is about 33% higher than that of the reference resonator. Recall that, due to hysteresis, in order to find R_c, the entire branch must be traced by incrementing the frequency Ω. The compression ratio reaches the value when the frequency is increased to 1.3123. The corresponding acceleration that achieves such a compression ratio has the amplitude $\tilde{A} = 6.6859\times10^{-4}$. According our assumption (8), accelerating the optimal resonator at this

acceleration and frequency consumes the same amount of input power that oscillates the reference conical resonator at $\tilde{A} = 5 \times 10^{-4}$ and its resonance frequency $\Omega = 1.3134$. As stated before, to find realistic dimensions of the resonator, the optimization scheme limits the lower bound for the dimensionless radius of the resonator at the narrow end to be $R(X = 0) =$ 0.020833. From the dimensions of the optimal conical resonator, the smaller narrow end, S_0, generates a larger compression ratio. Due to the fixed input-power constraint, the slope of the optimal cone S_1 is finite. The reference resonator and the optimal conical resonator are shown in Fig. 7. The second cone (Fig. 7(b)) has the smaller narrow end and smaller slope than the first (Fig. 7(a)).

D. Optimal horn-cone shapes

The horn-cone geometry used in this study is described by Eq. (10). The three shape parameters S_0, S_1 and S_2 are optimized. The first optimization attempt starts with the dimensions of the horn-cone given in Lawrenson *et al.*[1], $S_0 = 0.028333, S_1 = 5.7264$ and $S_2 = 0.25$. Using the original shape parameters, the compression ratio $R_c = 13.564$ is achieved when the horn-cone resonator is accelerated at $\tilde{A} = 5.0613 \times 10^{-4}$ and the frequency is increased to $\Omega = 1.4674$. In searching for the optimal horncone design, the lower bound of the radius of the narrow end S_0 is limited to be 0.020833 and the upper bound of S_1 to be 6 for practical reasons. The separation point between the horn section and the cone section, S_2, could be any value between 0 and 1. The result of optimization finds that the compression ratio reaches a

maximum value of 21.547, 58% higher than that of the horncone of Lawrenson *et al.*[1], when $S_0 = 0.20833, S_1 = 5.7263$ and $S_2 = 0.24893$. This optimal horncone achieves the value of the compression ratio when its acceleration has the amplitude $\tilde{A} = 5.9782 \times 10^{-4}$ and it is oscillating at its resonance frequency $\Omega = 1.4696$. These values of the acceleration and the frequency satisfy the requirement of fixed input power formulated in Eq. (8).

The optimization scheme BFGS is designed for finding a local extreme of a multivariable function. Our numerical simulations indicate that the compression ratio, as a function of the shape parameters, usually has many local extrema. Our second optimization attempt started with a different initial geometry of the horncone and a much higher value of the compression ratio $R_c = 40.203$ is obtained when $S_0 = 0.020833, S_1 = 5.5232$ and $S_2 = 0.22747$. For this compression ratio, the resonator is oscillated at the acceleration amplitude $\tilde{A} = 6.5817 \times 10^{-4}$ and the frequency $\Omega = 1.4259$. Comparing with the compression ratio for the horncone in Lawrenson *et al.*[1] (shown in Fig. 8(a)), the second optimal horncone (shown in Fig. 8(b)) improves the compression ratio by more than 196% at the same value of input power. For horncone shapes, the principle that higher compression ratio is obtained with smaller narrow end is valid, as in the case of conical shapes. Comparing the dimensions of the two horncones, the optimal horncone is smaller and the cone section is relatively longer than that of the horncone used in Lawrenson *et al.*[1]. In Fig. 8(c), the pressure waveform at the narrow end is presented for the two horncones. The waveform for the new horncone design is more complicated exhibiting two notable peaks per cycle. One pressure peak is significantly higher than the other. The two pressure waves corresponding to the two horn-cones also have different phases. Under the

prescribed conditions, the peak of the pressure is about 4.7 times the ambient pressure in the optimal horncone while the peak is about 3.2 times for the horncone in Lawrenson *et al.*[1].

E. Optimal cosine shape

The cosine shape is defined as

$$R(X) = S_0 + S_1(1-\cos(S_2 X)), \text{ for } 0 \le X \le 1 \tag{12}$$

Assuming the input power is entirely determined by the interior gas pressure, Chun and Kim[5] compared three individual resonators of the same volume: one conical shape, one ½-cosine shape ($S_2 = \pi$) and one ¾-cosine shape ($S_2 = 3\pi/2$). They found that the ½-cosine resonator produces the highest compression ratio among the three resonators. Starting with the ½-cosine dimensions reported in Chun and Kim[5], $S_0 = 0.025, S_1 = 0.095, S_2 = \pi$, all three shape parameters are optimized using our criteria. The resulting optimal cosine shape parameters are given by $S_0 = 0.020833$, $S_1 = 0.073545$ and $S_2 = 3.2603$, and the resonator shape is shown in Fig. 9(b). For the optimal shape, we obtain the compression ratio $R_c = 13.693$ at the frequency $\Omega = 1.4830$, which is about 20% better than that of Chun and Kim[5] at the same level of input power. Using different initial guesses of shape parameters for cosine resonators, the optimization scheme produced results that yielded lower compression ratios.

Under the specified conditions (the same power input $<W_1>$, the ratio of specific heats γ and the viscosity-related parameter G), the horn-cone shape is found to be better than the cosine shape in generating higher compression ratio at the narrow end, opposite the findings of Chun

and Kim[5]. As shown in Fig. 9(c), the pressure waveform of the optimal cosine design is similar to that of Chun and Kim[5] with a greater pressure peak and a different phase.

V. CONCLUSIONS

A local optimization scheme is presented for finding the resonator shapes that maximize the pressure compression ratio at one end of an oscillating acoustic resonator. The optimal dimensions are reported for cone, horncone, and cosine shaped resonators. The results are summarized in Table I, including the shape parameters, corresponding acceleration amplitude, resonance frequency, and compression ratio.

For each type of resonator, a smaller narrow end is found to give a larger pressure peak-to-peak ratio. This finding suggests that the number of shape parameters in an optimization can be reduced by setting the dimension of the narrow end fixed at a value as small as possible. For the types of horncone and cosine shapes, there are many different designs that achieve local extrema. Using different initial guesses for the optimal design, the results show that as much as 196% improvement on the compression ratio can be achieved with a fixed level of input power. For the shapes considered herein, the horncone shape is found to generate the highest compression ratio. The acoustic field in a resonator is a continuous function of the resonator shape, the ratio of specific heats and the viscosities. Consequently, the dimensions of optimal resonator shape reported herein will undergo small changes if ratio of specific heats and/or the viscosities change by a small amount. Searching strategies for globally optimal shapes are under investigation.

REFERENCES

[1]C. C. Lawrenson, B. Lipkens, T. S. Lucas, D. K. Perkins, and T. W. Van Doren, "Measurements of macrosonic standing waves in oscillating closed cavities." J. Acoust. Soc. Am. **104**, 623-636 (1998).

[2]Y. A. Ilinskii, B. Lipkens, T. S. Lucas, T. W. Van Doren, and E. A. Zabolotskaya, "Nonlinear standing waves in an acoustical resonator," J. Acoust. Soc. Am. **104**, 2664-2674 (1998).

[3]Y. A. Ilinskii, B. Lipkens and E. A. Zabolotskaya, "Energy losses in an acoustical resonator," J. Acoust. Soc. Am. **109**, 1859-1870 (2001).

[4]M. F. Hamilton, Y. A. Ilinskii, and E. A. Zabolotskaya, "Linear and nonlinear frequency shifts in acoustical resonators with varying cross sections," J. Acoust. Soc. Am. **110**, 109-119 (2001).

[5]Y.-D. Chun and Y.-H. Kim, "Numerical analysis for nonlinear resonant oscillations of gas in axisymmetric closed tubes." J. Acoust. Soc. Am. **108**, 2765-74 (2000).

[6]R. R. Erickson and B. T. Zinn, "Modeling of finite amplitude acoustic waves in closed cavities using the Galerkin method," J. Acoust. Soc. Am. **113**, 1863-70 (2003).

[7]X. Li, J. Finkbeiner, G. Raman, C. Daniels, and B. Steinetz, "Nonlinear resonant oscillations of gas in optimized acoustical resonators and the effect of central blockage", AIAA paper No. 2003-0368, *41st AIAA Aerospace Sciences Meeting and Exhibit* 2003 Reno, Neveda.

[8]P. E. Gill, W. Murray, and M. H. Wright, *Practical Optimization* (Academic Press, New York, 1981).

[9]J. Finkbeiner, X. Li, C. Daniels, G. Raman, and B. Steinetz, "Effect of forcing function on nonlinear acoustic standing waves", *145th Meeting of the Acoustical Society of America* May 2003, Nashville, TN.

[10]C. Daniels, J. Finkbeiner, B. Steinetz, X. Li, and G. Raman, "Determination of dimensionless attenuation coefficient in shaped resonators", presentation 4aPAa3, *145th Meeting of the Acoustical Society of America* May 2003, Nashville, TN.

Table I. **Summary of the optimization. The shape parameters of the resonators in previous studies and the optimized resonators and their compression ratios are listed. The corresponding acceleration levels and oscillating frequencies that achieve the compression ratios are also shown.**

	S_0	S_1	S_2	$\tilde{A}$ (x10^{-4})	Ω	R_c
Cone:						
Ilinskii, *et al.*	0.032941	0.268	N/A	5.0	1.3134	5.0475
Optimal	0.020833	0.15438	N/A	6.6859	1.3123	6.7213
Horn-cone:						
Lawrenson, *et al.*	0.028333	5.7264	0.25	5.0613	1.4674	13.564
Optimal	0.020833	5.5232	0.22747	6.5817	1.4259	40.203
Cosine-shape:						
Chun and Kim	0.025	0.095	3.1416	5.6299	1.4837	11.440
Optimal	0.020833	0.073545	3.2603	5.0613	1.4830	13.693

Figure Captions

Figure 1. The reduced pressure p/p_0 at the ends of a horncone and a cylinder at their corresponding resonance frequencies for the same acceleration $\tilde{A} = 1 \times 10^{-3}$.

Figure 2. The ratio between the amplitudes of the second and the first harmonics of the pressure wave, p_2/p_1, is plotted as a function of the dimensionless amplitude of the first harmonic reduced pressure p_1/p_0. These amplitudes are calculated for the narrow end of the horncone and at one end of the cylinder.

Figure 3. The effect of the frequency and the amplitude of acceleration on the dimensionless amplitude of the first harmonic reduced pressure p_1/p_0. The pressure is calculated for the narrow end of the horncone for the acceleration $\tilde{A} = 2 \times 10^{-4}$ (crosses) and $\tilde{A} = 1 \times 10^{-3}$ (circles and squares).

Figure 4. Experimental apparatus.

Figure 5. The dimensionless acceleration signals measured at the two ends of the horncone resonator by PCB accelerometers.

Figure 6. The dynamic pressure frequency response measured at the narrow end of the horn-cone resonator and the pressure responses predicted by the numerical model computed for varying

values of G with a dimensionless acceleration level, $\tilde{A} = 1.03 \times 10^{-4}$, matching the acceleration measured at the resonator narrow end.

Figure 7. Conical shapes: (a) the reference conical resonator; (b) the optimized conical resonator. For the same input power, the compression ratios corresponding to the shapes in (a) and (b) reach the values of 5.0475 and 6.7204 respectively. For shape parameters, see the text.

Figure 8. (a) The horncone shape in Lawrenson *et al.*[1] (b) Optimized horncone shape. For shape parameters, see the text. (c) The pressure waveform at the narrow end for the horncone in Lawrenson *et al.*[1] (the solid line) and that for the second optimized horncone (the dashed line) are shown.

Figure 9. (a) The ½-cosine shape as in Chun and Kim[5]. (b) The optimized ½-cosine shape. (c) The pressure waveform at the narrow end for the ½-cosine resonator in Chun and Kim[5] (the solid line) and that for the optimized ½-cosine shape (the dashed line) are shown.

Figure 1

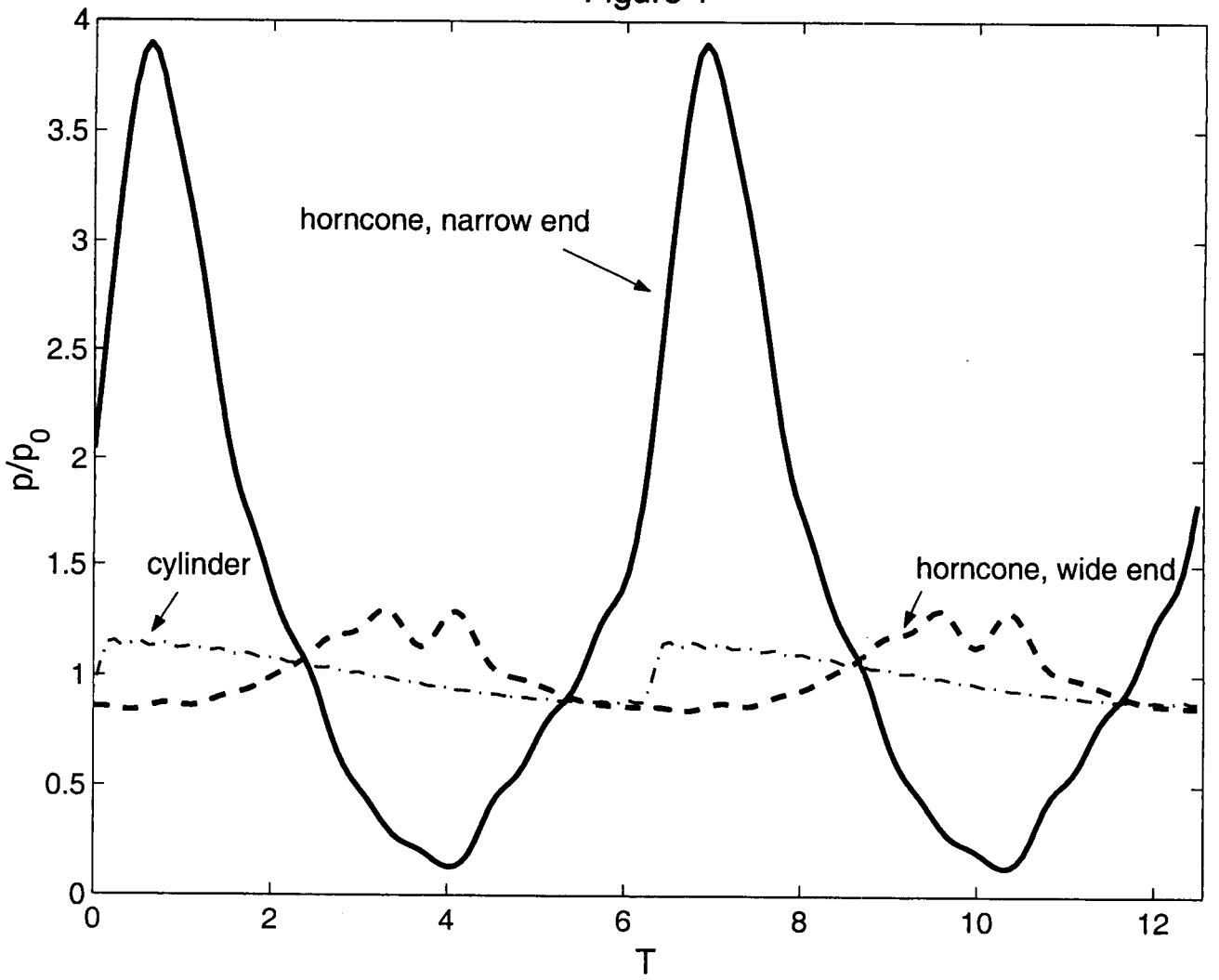
4
3.5
3
2.5
2
1.5
1
0.5
0
0
2
4
6
8
10
12
p/p0
T
horncone, narrow end
cylinder
horncone, wide end

Figure 2

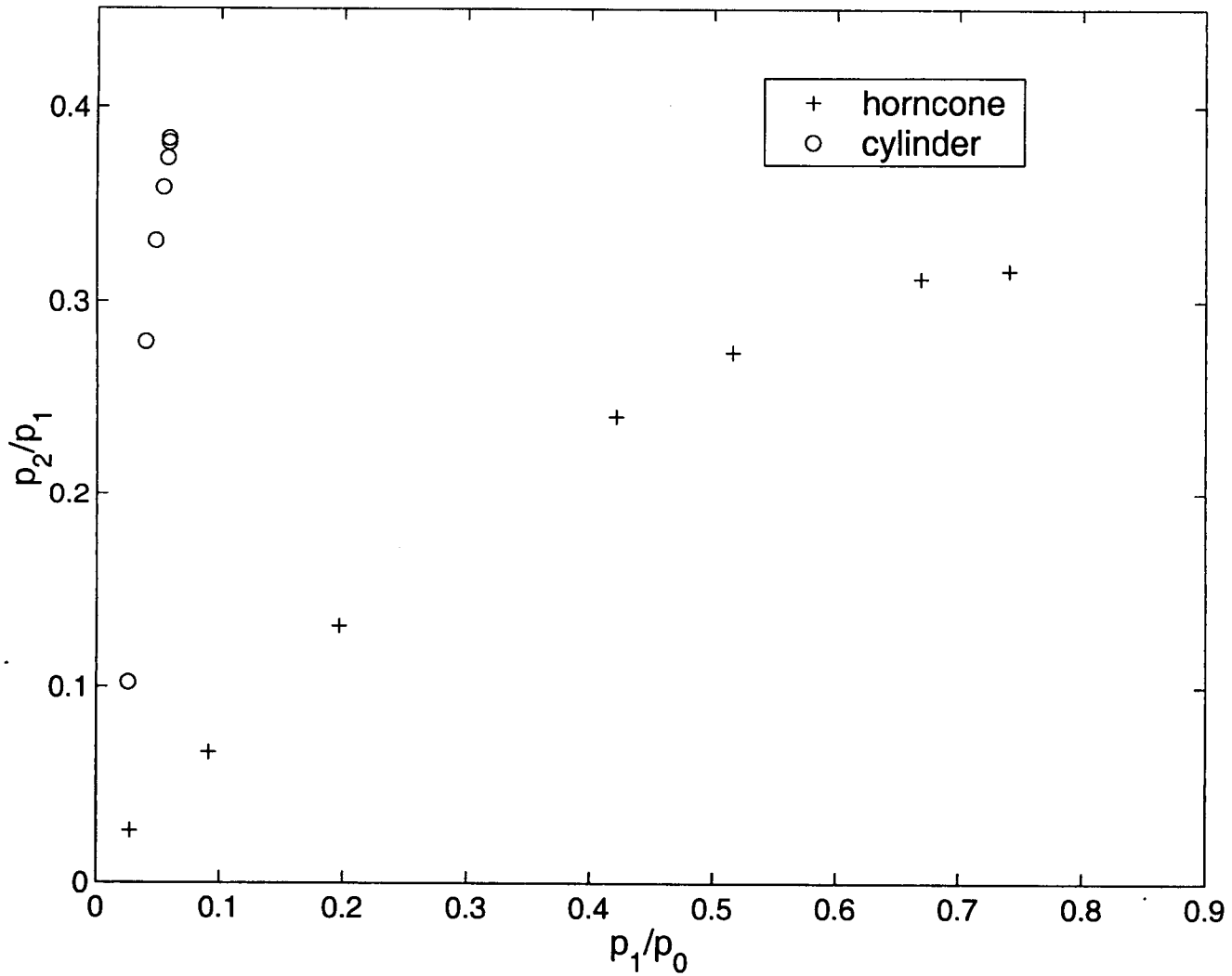
horncone
cylinder
0.4
0.3
0.2
0.1
0
p_2/p_1
0
0.1
0.2
0.3
0.4
0.5
0.6
0.7
0.8
0.9
p_1/p_0

Figure 3

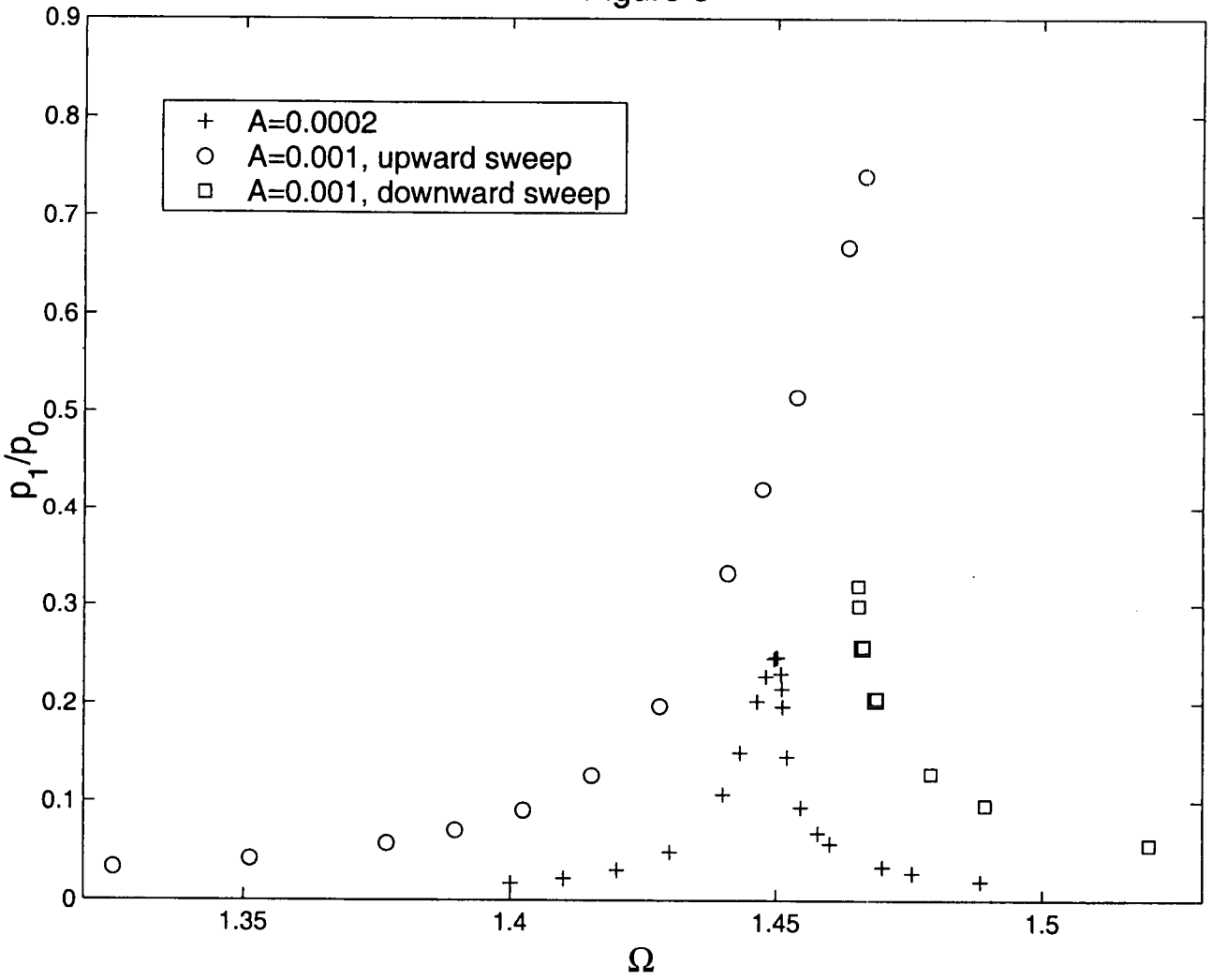
A=0.0002
A=0.001, upward sweep
A=0.001, downward sweep
p_1/p_0
Ω
0
0.1
0.2
0.3
0.4
0.5
0.6
0.7
0.8
0.9
1.35
1.4
1.45
1.5

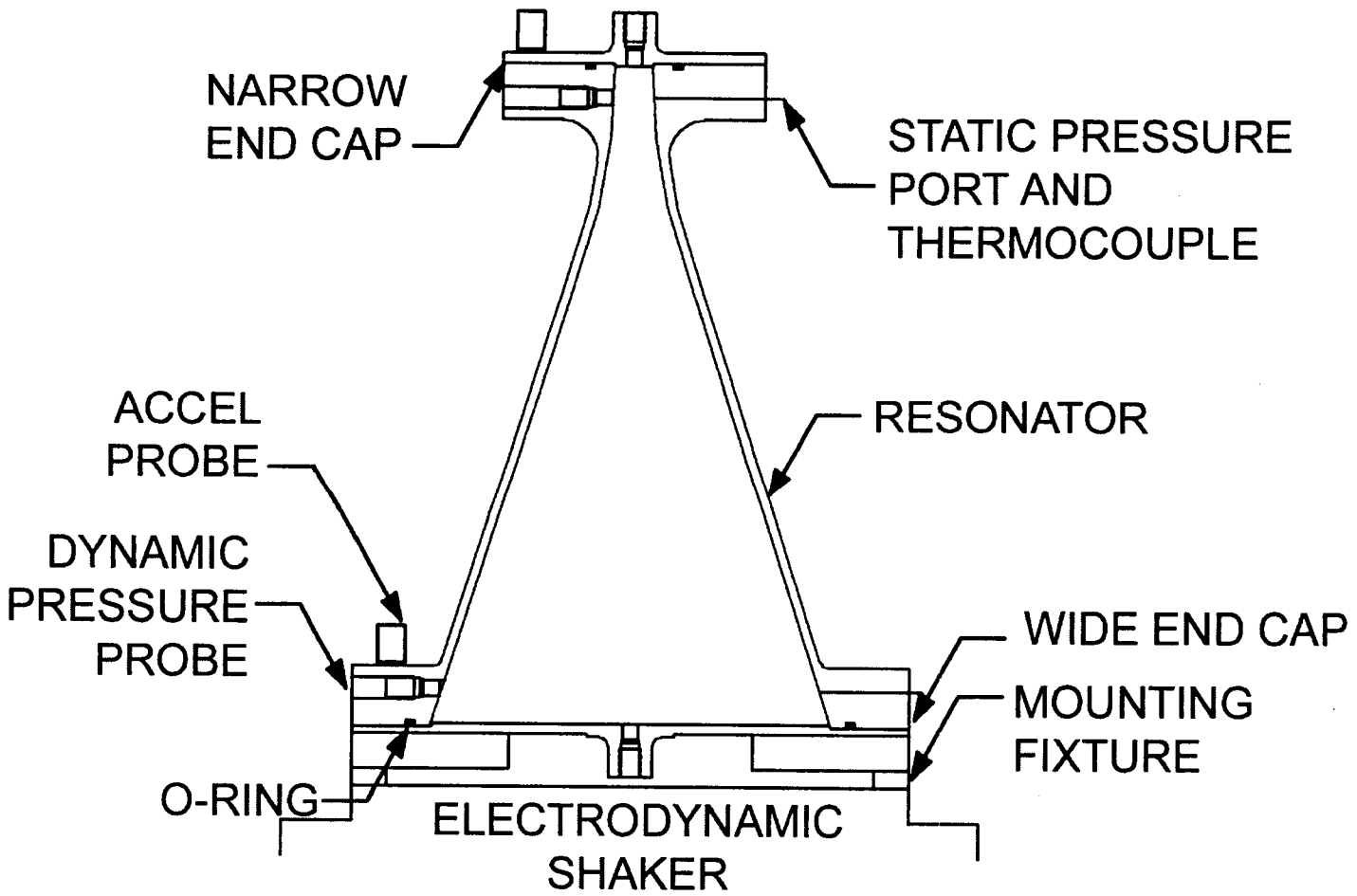
NARROW
END CAP
STATIC PRESSURE
PORT AND
THERMOCOUPLE
ACCEL
PROBE
RESONATOR
DYNAMIC
PRESSURE
PROBE
WIDE END CAP
MOUNTING
FIXTURE
O-RING
ELECTRODYNAMIC
SHAKER

Figure 5

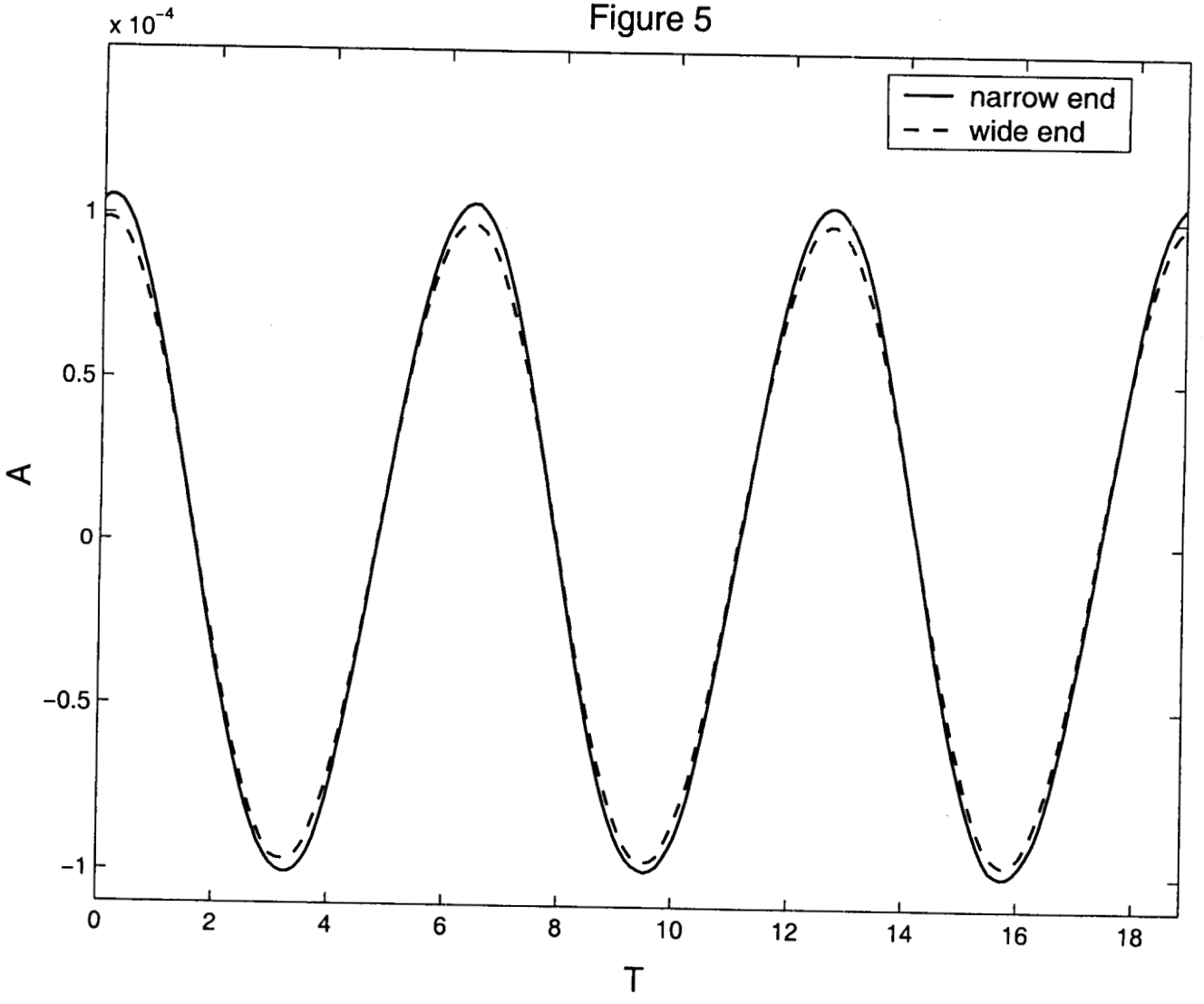

Figure 6

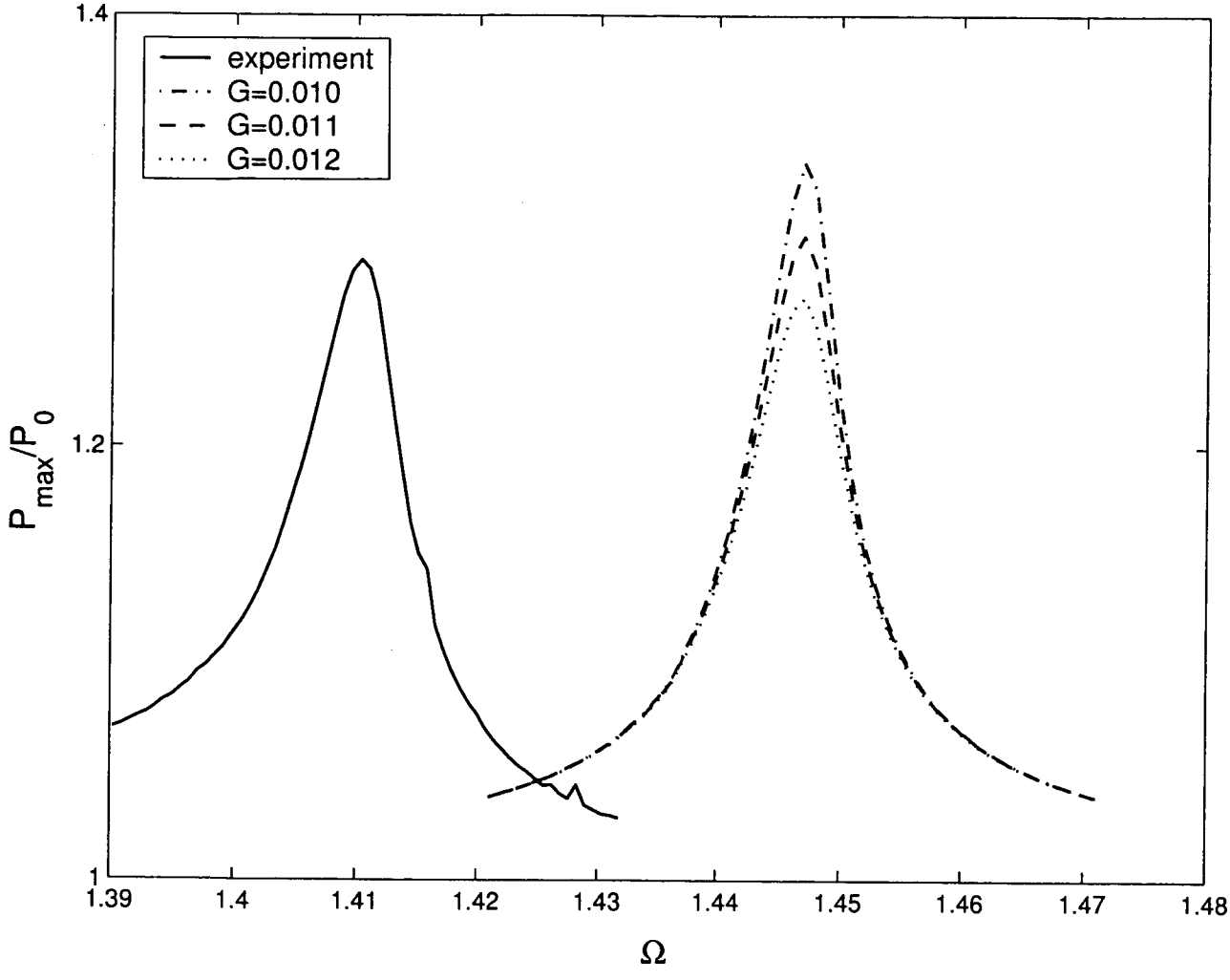
experiment
G=0.010
G=0.011
G=0.012
1.4
1.2
1
1.39
1.4
1.41
1.42
1.43
1.44
1.45
1.46
1.47
1.48
P_{max}/P_0
Ω

Figure 7

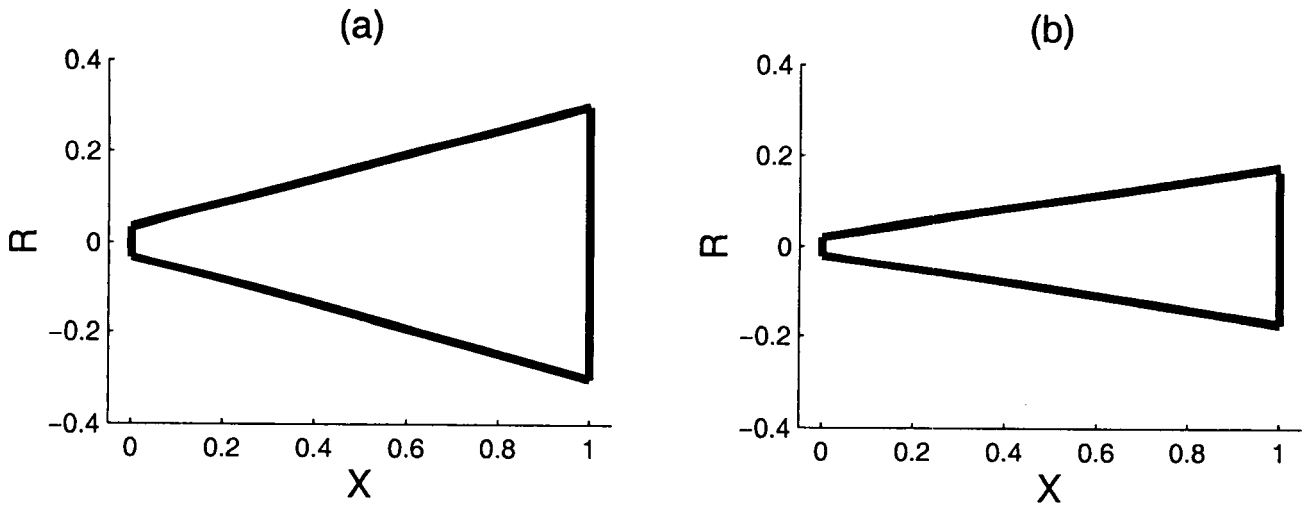

Figure 8

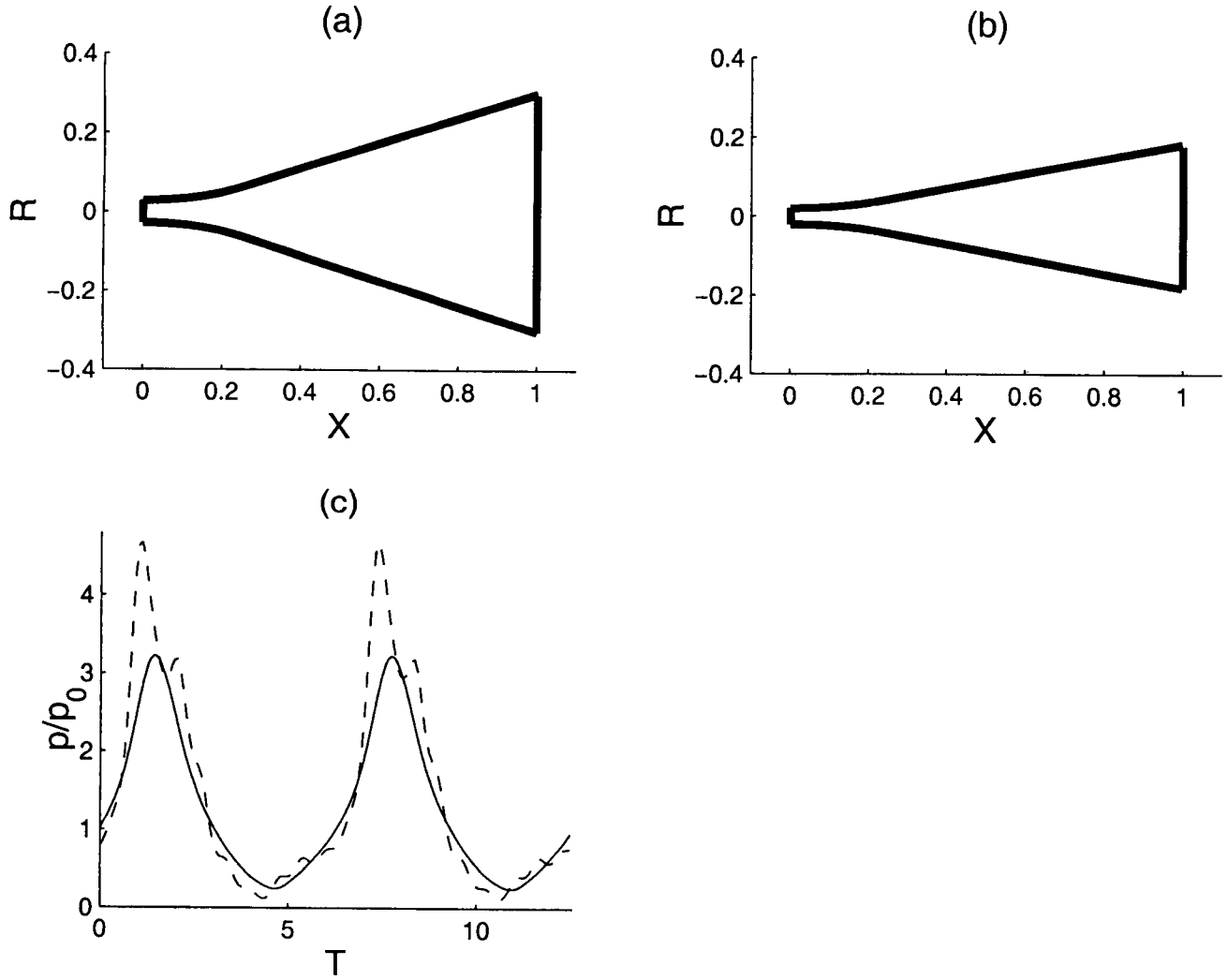
(a)
0.4
0.2
0
−0.2
−0.4
R
0
0.2
0.4
0.6
0.8
1
X
(b)
0.4
0.2
0
−0.2
−0.4
R
0
0.2
0.4
0.6
0.8
1
X
(c)
4
3
2
1
0
p/p0
0
5
10
T

Figure 9

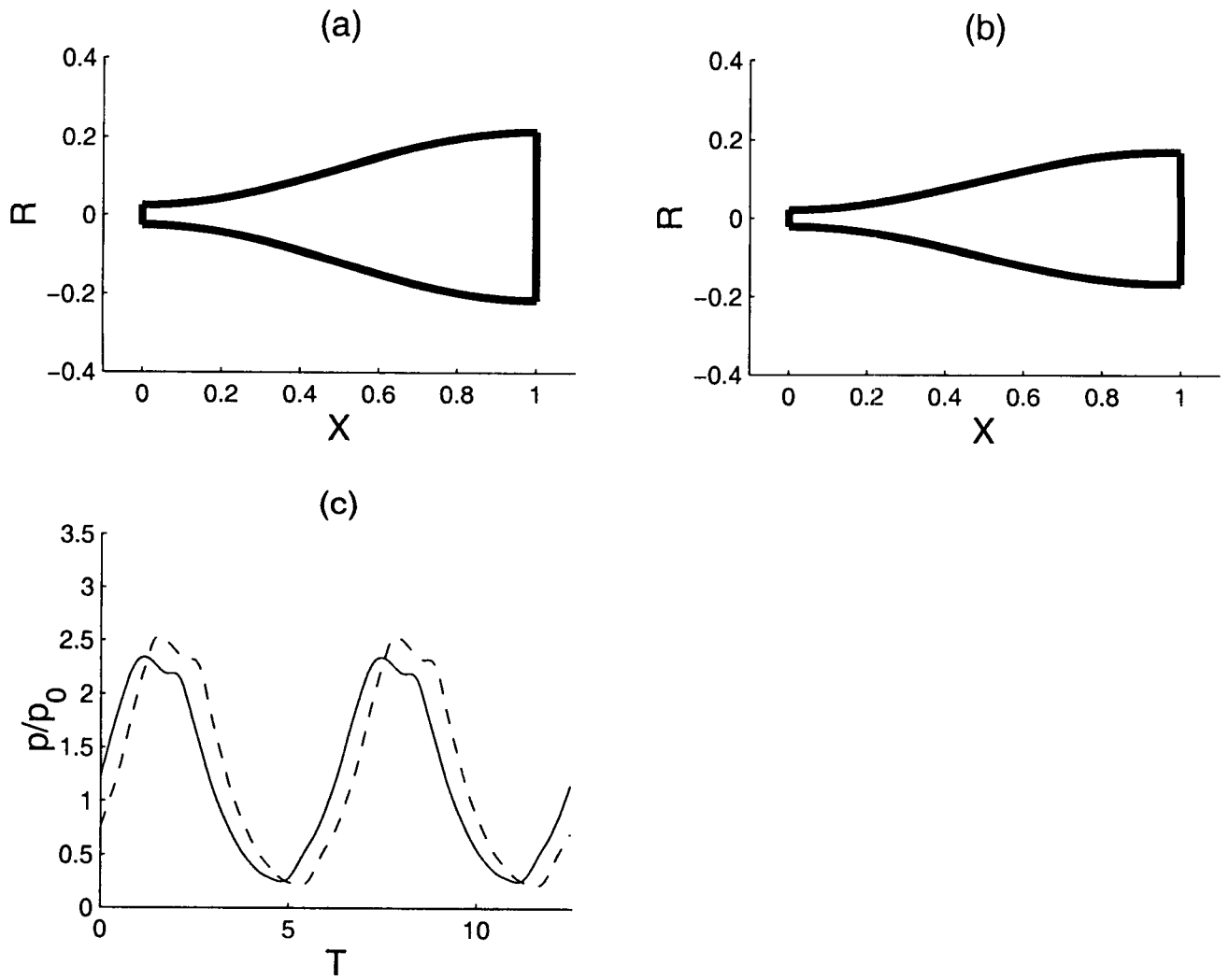
(a)
0.4
0.2
0
−0.2
−0.4
R
0
0.2
0.4
0.6
0.8
1
X
(b)
0.4
0.2
0
−0.2
−0.4
R
0
0.2
0.4
0.6
0.8
1
X
(c)
3.5
3
2.5
2
1.5
1
0.5
0
p/p0
0
5
10
T